Bipolar-variant spin angular momentum and its evolution in a tight focusing process

Xu-Zhen Gao (高旭珍), Jia-Hao Zhao (赵嘉豪), Meng-Shuai Wang (王梦帅), Jin-Jin Liu (刘进进), Guang-Bo Zhang (张广博), and Yue Pan (潘岳)*

School of Physics and Physical Engineering, Shandong Provincial Key Laboratory of Laser Polarization and Information Technology, Qufu Normal University, Qufu 273165, China

(Received 25 June 2020; revised 23 September 2020; accepted 2 November 2020; published 10 December 2020)

We design and generate the bipolar-variant spin angular momentum (SAM) carried by vector optical field and theoretically investigate the evolution of the bipolar-variant SAM in the tight focusing process. It is found that the longitudinal SAM density annihilates and the purely transverse SAM density appears in the focal plane, and the evolution of the complex singularities of SAM into V-point singularities is also studied. We further extend the study to general bipolar-variant SAM, and give the theoretical explanation of the annihilation and appearance of different components of SAM density. We believe the presentation of the bipolar-variant SAM can greatly enrich the study of SAM as well as the singular optics. Meanwhile, the evolution of the bipolar-variant SAM in the focusing process is interesting and important in revealing the focal properties of SAM of the photon, and the purely transverse SAM in the focal plane with a spin axis orthogonal to the propagation direction opens up avenues in optical trapping and manipulation, especially for optically induced rotations.

DOI: 10.1103/PhysRevA.102.063514

I. INTRODUCTION

Polarization and phase are two important salient features of light, and they are both associated with angular momentum (AM): spin angular momentum (SAM), and orbital angular momentum (OAM), respectively. As an intrinsic nature of the light field, OAM is associated with the vortex phase of structured light and can make the particle orbit around the optical axis [1–6]. Meanwhile, SAM is related to the circular polarizations with two possible quantized values of $\pm\hbar$, which can make the particle spin around its own axis [3,4,7,8]. Traditional SAM density is either parallel or antiparallel to the propagation direction of the optical field, which is called the longitudinal SAM density. Recently, the transverse SAM density, which is perpendicular to the propagation direction, has attracted extensive attention [9–12]. The transverse SAM is also known as the photonic wheel [11], which allows for additional rotation degrees of freedom in optical manipulation, as it can rotate the particle along a nonaxial direction [10–16]. Along with increasing interest in studying the vector optical fields (VOFs) with space-variant states of polarization (SoPs) [17–22], VOFs are widely used in generating transverse SAM, as they can lead to strong longitudinal component of the tightly focused field [11–13,16,23–26]. However, the generation of transverse SAM by tightly focusing VOF without cylindrical symmetric SAM distribution is rarely reported.

In this paper, we present the bipolar-variant SAM carried by noncylindrical symmetric VOF in bipolar coordinates and achieve purely transverse SAM in the focal plane. We further extend the concept to general bipolar-variant SAM and discuss the varying singularity structure. Moreover, the annihilation of longitudinal SAM and appearance of the transverse SAM in a tight focusing process are explained theoretically. We hope the transition from longitudinal to transverse SAM can bring insights into SAM evolution and that the purely transverse SAM in the focal plane can hold potential applications in various areas including nanophotonics, quantum processing, and biophotonics.

II. THE DESIGN AND GENERATION OF BIPOLAR-VARIANT SAM CARRIED BY VOF

As is well known, the VOF with hybrid SoP consists of linear, elliptical, and circular polarizations on the wavefront simultaneously [27–30], which can lead to the space-variant SAM distribution. Specially, for the VOF with hybrid SoP designed in the polar coordinates [27,28], the SAM varying along the azimuthal direction can be regarded as the azimuthal-variant SAM. In contrast with the famous OAM originated from azimuthally variant phase distribution, the azimuthal-variant SAM is interesting to study as it originated from azimuthally variant polarization distribution. Figure 1(a) shows the polar coordinate system, and the constant curves of the two coordinates (ρ, φ) are presented as an orange solid circle and purple dashed ray, respectively. The SoP of the VOF carrying azimuthal-variant SAM designed in the polar coordinates is shown in Fig. 1(b), and the SoP keeps the same along the constant φ curve and changes along the constant ρ curve.

By analogy with the azimuthal-variant SAM, we propose a bipolar-variant SAM carried by VOF. The scheme of the bipolar coordinate system is shown in Fig. 1(c) and the constant u and v curves are two groups of nonconcentric circles, respectively. The bipolar coordinates (u, v) have the following

*panyue.89@163.com, panyue@qfnu.edu.cn

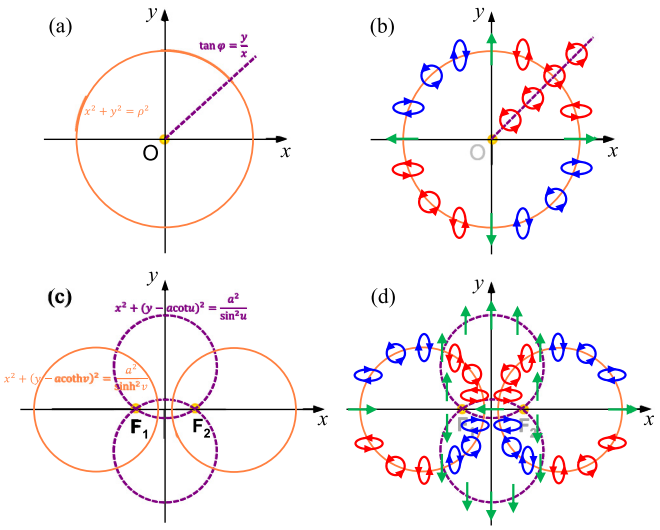

FIG. 1. (a) The polar coordinate system where the purple dashed ray and orange solid ring represent the constant curves of the polar coordinates φ and ρ, respectively. (b) The SoP of VOF carrying azimuthal-variant SAM in polar coordinate system. (c) The bipolar coordinate system where the purple dashed and orange solid curves represent the constant curves of the bipolar coordinates u and v, respectively. (d) The SoP of the VOF carrying bipolar-variant SAM in bipolar coordinate system when $m = 1$. Red ellipse: Right-handed elliptic (circular) polarization; blue ellipse: left-handed elliptic (circular) polarization; green arrow: linear polarization.

relationship with the Cartesian coordinates (x, y) [31]:

$$x^2 + (y - a\cot u)^2 = \frac{a^2}{\sin^2 u}, \tag{1a}$$

$$x^2 + (y - a\coth v)^2 = \frac{a^2}{\sinh^2 v}, \tag{1b}$$

where $2a$ is the focal length of the two foci in bipolar coordinate system located at $(-a, 0)$ and $(a, 0)$, which are represented as the yellow dots in Fig. 1(c).

The SoP of the VOF carrying bipolar-variant SAM is shown in Fig. 1(d), and the polarizations keep the same along the constant u curve and change along the constant v curve. The electric field distribution of the VOF carrying bipolar-variant SAM can be expressed as

$$\mathbf{E}(u) = \cos(mu)\hat{\mathbf{e}}_x + j\sin(mu)\hat{\mathbf{e}}_y, \tag{2}$$

where $\{\hat{\mathbf{e}}_x, \hat{\mathbf{e}}_y\}$ are the unit vectors in Cartesian coordinates. m is the topological charge of the bipolar-variant SAM, which can control the changing period of SAM around one focus of the bipolar coordinates. To study the bipolar-variant SAM in more detail, we calculate the time-averaged SAM density of this VOF as [32–36]

$$\mathbf{S} = \frac{\mathrm{Im}\left[\varepsilon(\mathbf{E}^* \times \mathbf{E}) + \mu(\mathbf{H}^* \times \mathbf{H})\right]}{4\omega}, \tag{3}$$

where ω is the angular frequency of the field, ε and μ are the vacuum permittivity. Im[·] represents the imaginary parts, and $\mathbf{E}^*$ and $\mathbf{H}^*$ denote the complex conjugate of the electric and magnetic fields, respectively. We consider the cases in free space with nonmagnetic surrounding medium, so only the SAM originated from the electric field is taken into account. The three components of the SAM density can be expressed as

$$S_x = \frac{\varepsilon}{4\omega}\mathrm{Im}[E_y^* E_z - E_z^* E_y],$$
$$S_y = \frac{\varepsilon}{4\omega}\mathrm{Im}[E_z^* E_x - E_x^* E_z],$$
$$S_z = \frac{\varepsilon}{4\omega}\mathrm{Im}[E_x^* E_y - E_y^* E_x]. \tag{4}$$

For the VOF-carrying bipolar-variant SAM we propose, the transverse components of the SAM density S_x and S_y are zero in the incident plane, which is associated with the zero longitudinal component of the electric field, as recognized from Eq. (4). The longitudinal SAM density is $S_z = \frac{\varepsilon}{4\omega}\sin(2mu)$, which keeps the same along the constant u curves (two series of purple circles) and changes along the constant v curves (two series of orange circles), as shown in Figs. 1(c) and 1(d).

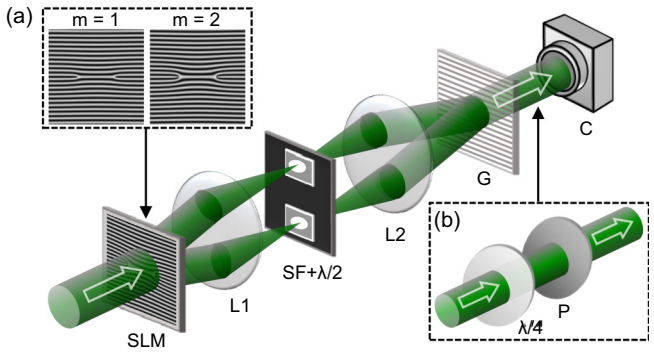

FIG. 2. Experimental setup. SLM, spatial light modulator; L1 and L2, lenses; SF, spatial filter; $\lambda/2$ and $\lambda/4$, half- and quarter-wave plates; G, Ronchi phase grating; C, camera; P, polarizer. The inset (a) depicts two holographic gratings with $m = 1$ and 2. (b) shows the setup used to probe the polarization state of the generated VOF carrying bipolar-variant SAM.

To experimentally generate the VOF carrying bipolar-variant SAM, a common path interferometer implemented with a spatial light modulator (SLM) and a $4f$ system are employed [28,31,37–40], as shown in Fig. 2. The input collimated beam is split into $\pm$1st orders via a bi-fork holographic grating loaded in the SLM with 1920×1024 pixels (each pixel has a dimension of $8\times8\,\mu\mathrm{m}^2$). The holographic grating is composed of two forks with different locations, and the number of the forking shape in each fork is determined by m, as shown in Fig. 2(a). The diffracted $\pm$1st orders are allowed to pass through a spatial filter and then are converted into two orthogonally $\pm45^\circ$ linearly polarized beams by a pair of half-wave plates located at the Fourier plane of the $4f$ system. The two orthogonally linearly polarized parts are recombined by the Ronchi phase grating placed in the output plane of the $4f$ system. The setup composed of a quarter-wave plate and a polarizer is used to probe the stokes parameters of the generated VOF carrying bipolar-variant SAM, as shown in Fig. 2(b). We should point out that we use another $4f$ system

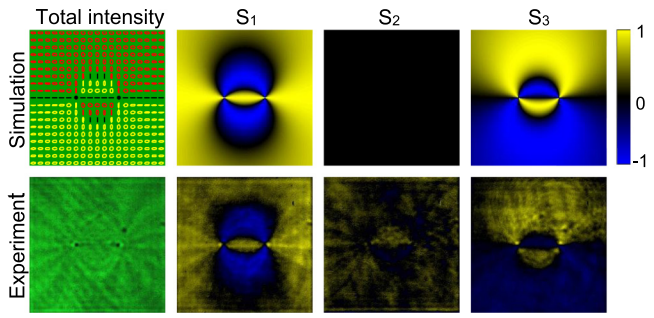

FIG. 3. The simulated and measured total intensity patterns and normalized Stokes parameters of the VOF carrying bipolar-variant SAM when $m = 1$ and $a = 0.3\rho_m$, where ρ_m is the radius of the VOF. The corresponding polarization distribution is superimposed with simulated intensity pattern in the first column. Red ellipse: Right-handed elliptic (circular) polarization; yellow ellipse: left-handed elliptic (circular) polarization; black line: linear polarization. The size of any pattern is 2.2 mm×2.2 mm.

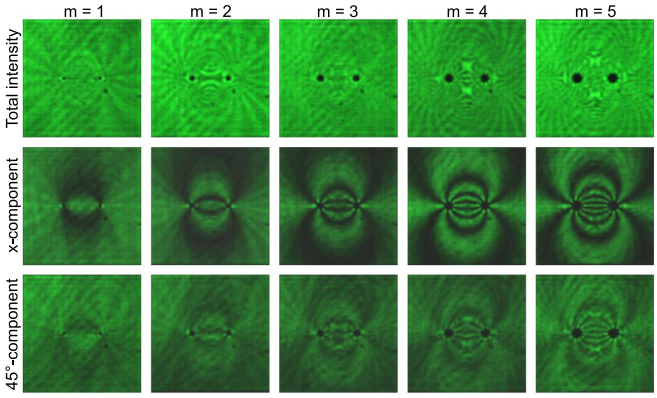

FIG. 4. Generated VOFs carrying bipolar-variant SAM when $a = 0.3\rho_m$, $m = 1, 2, 3, 4$, and 5, respectively. The first row shows the total intensity patterns, and second and third rows show the intensity patterns of the x and 45° components, respectively. The size of any pattern is 2.2 mm×2.2 mm.

in the experiment between the Ronchi phase grating and the camera to guarantee the quality of the VOF we generate.

Figure 3 shows the theoretically simulated and experimentally measured intensity patterns and normalized Stokes parameters of the VOF carrying bipolar-variant SAM when $m = 1$ and $a = 0.3\rho_m$, where ρ_m is the radius of the VOF. From the total intensity pattern, we can see that there are two singular spots located at two foci in the bipolar coordinate system, which is obviously different from the traditional cylindrical VOF with one central singularity. It is found that the measured Stokes parameter S_2 in Fig. 3 is in disagreement with the theoretical result, which is caused by the quarter-wave retarder plate and polarizer used to measure the Stokes parameters in the experiment as shown in Fig. 2(b). Specifically, the lack of precision in their orientation to probe S_2 and the slight wavelength difference of the incident field and the wave plate lead to this discrepancy. The Stokes parameters S_1 and S_3 exhibit the similar shapes as the constant u curves, which are in good agreement with the theoretical simulations. Note that the Stokes parameter S_3 is proportional to the longitudinal SAM density by the formula $S_3 = j(E_x E_y^* - E_y E_x^*) = \sin(2mu) \propto S_z$. As a result, the Stokes parameter S_3 can represent the longitudinal component of the SAM density S_z. We can find clearly from Fig. 3 that the longitudinal SAM keeps the same along the constant u curve, which agrees with the discussion in Fig. 1, proving that the generated VOF carries bipolar-variant SAM.

Recently, the polarization singularity has attracted interest in recent years [41,42]. The V point is defined as the point where the direction of the polarization vector is undefined at the beam center and the C point is the isolated point of circular polarization where the orientation of the major axis of polarization ellipse is undefined. The L line is the line connecting points where the handedness of polarization ellipse is undefined. According to the SoP of the VOF carrying bipolar-variant SAM in Fig. 1(d), the singularities here at the two foci of the bipolar coordinate system are complex polarization singularities where the orientation, ellipticity, and handedness of the polarization ellipse are all undefined simultaneously. It is also obvious that the longitudinal SAM, proportional to the Stokes parameter S_3, is undefined at the two foci in the bipolar coordinate system, as shown in Fig. 3. Therefore, we name these singularities as complex singularities of the SAM where the SAMs are undefined, which is different from the traditional polarization singularities.

Figure 4 shows the generated VOFs carrying bipolar-variant SAM when the topological charge $m = 1, 2, 3, 4$, and 5, respectively. The total intensity patterns exhibit uniform distribution excluding two singularities. The experimentally measured singularities become bigger as m increases, mainly because the SLM with limited resolution cannot distinguish the rapidly changing polarizations and the polarizations are more complex around the two singularities when m increases. Meanwhile, the fixed aperture of the 4f imaging system and the size of the spatial filter can also result in different sizes of singularities, as they will lead to the loss of high-order spatial modes during imaging. We should also point out that in theory, the singularities should be geometric points independent of m. The extinction circles or light-passing circles of the intensity patterns of the x component always pass though the two complex singularities and their number is equal to the value of m. It can also be seen that the points with the same polarization lie always in a constant u circle passing through the two foci, as shown in Fig. 1(c). The intensity patterns of the 45° components have no obvious extinction except the singularities and the intensity are a half of the total intensity.

III. THE EVOLUTION OF BIPOLAR-VARIANT SAM IN A TIGHT FOCUSING PROCESS

After generating a bipolar-variant SAM carried by VOF, we concentrate on studying the evolution property of the bipolar-variant SAM in the tight focusing process. According to the Richards-Wolf vectorial diffraction theory [43,44], the tightly focused VOF carrying bipolar-variant SAM can be

written as

$$\mathbf{E} = -\frac{jkf}{2\pi}\int_0^{\theta_m} d\theta \int_0^{2\pi} d\varphi P(\theta)\mathbf{M}e^{jk(z\cos\theta + r\sin\theta\cos(\phi-\varphi))}\sin\theta, \tag{5}$$

with

$$\mathbf{M} = \begin{bmatrix} [\cos(mu)(\cos\theta\cos^2\varphi + \sin^2\varphi) + j\sin(mu)\sin\varphi\cos\varphi(\cos\theta - 1)]\hat{\mathbf{e}}_x \\ [\cos(mu)\sin\varphi\cos\varphi(\cos\theta - 1) + j\sin(mu)(\cos\theta\sin^2\varphi + \cos^2\varphi)]\hat{\mathbf{e}}_y \\ [\cos(mu)\sin\theta\cos\varphi + j\sin(mu)\sin\theta\sin\varphi]\hat{\mathbf{e}}_z \end{bmatrix}, \tag{6}$$

where (ρ, φ) are the radial and azimuthal coordinates in the incident plane. r, ϕ, and z are the radial, azimuthal, and longitudinal coordinates in the focal plane. $k = 2\pi/\lambda$ is the wave vector of light with a wavelength of λ in free space. f is the focal length of the objective. $\theta_{\max} = \arcsin(\mathrm{NA})$ is the maximum ray angle through the objective lens, and NA is the numberical aperture of the focal lens. $P(\theta)$ is the pupil plane apodization function, which can be chosen as $P(\theta) = \sqrt{\cos\theta}$. Based on the derived electric field components in the focal plane, we can further calculate the time-averaged SAM density of the tightly focused field. Considering the nonzero contributions of the longitudinal component of tightly focused VOF, the transverse component of the SAM density may appear in the focal plane.

Figure 5 shows the variation of the SAM density of the VOF carrying bipolar-variant SAM in the tight focusing process when $a = 0.3\rho_m$ and $m = 1$. The SoP and longitudinal SAM density of the incident VOF carrying bipolar-variant SAM are shown in Figs. 5(a) and 5(b), respectively. It is obvious that the SoP and longitudinal SAM density S_z keep the same along the constant u curve, and the longitudinal SAM density is symmetric about the y axis and opposite about the x axis. The corresponding intensity patterns and the SAM densities in the tight focusing plane with the numerical aperture NA = 0.95 are shown in Figs. 5(c)–5(h). From the SoP superimposed with the transverse focal intensity pattern in Fig. 5(d), we can find that the transverse field is purely linearly polarized in the focal plane. This indicates that the local polarizations undergo an absolute transition from elliptical (circular) polarizations to linear polarizations in the focusing process. The two singularities in the focal plane are shown by the white dots in Fig. 5(d), which are obviously V points as the orientations of linear polarizations at these two positions are undefined. Figures 5(f)–5(h) illustrate the x, y, and z components of the SAM density in the focal plane, which is normalized by the maximum value of S'_x. It is obvious that the longitudinal SAM density annihilates and purely transverse SAM density appears in the focal plane. As a result, a particle trapped in such a focused field is expected to rotate along a nonaxial direction, which provides additional rotational degrees of freedom in optical manipulation.

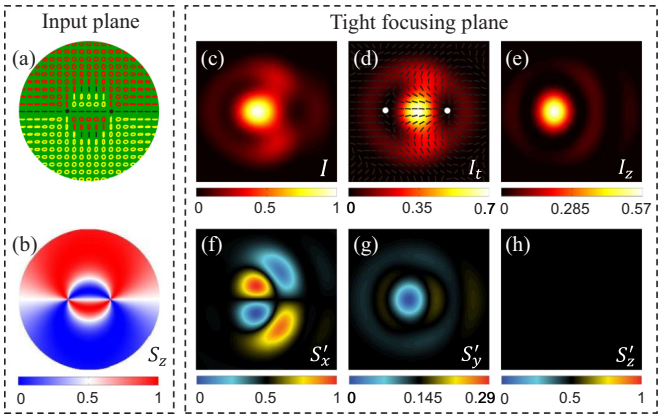

FIG. 5. (a) The polarization distribution and (b) longitudinal SAM density distribution of the VOF carrying bipolar-variant SAM with $m = 1$ and $a = 0.3\rho_m$ in the input plane. (c)–(e) The total intensity I, transverse intensity I_t, and longitudinal intensity I_z of the tightly focused VOF carrying bipolar-variant SAM when NA = 0.95. The corresponding SoP is superimposed with the transverse intensity pattern in (d) and the white dots indicate polarization singularities. (f)–(h) Three components of the SAM density in the tight focusing plane. Any image in the focusing plane has a dimension of $2.5\lambda \times 2.5\lambda$.

To investigate the influence of the topological charge m on the variation of the bipolar-variant SAM during a tight focusing process, we further discuss the case when $m = 2$ in Fig. 6. Compared with the case in Fig. 5, the changing period of the SoP and SAM is two times larger when $m = 2$ and the energy distribution of the tightly focused field also changes. Moreover, we find that the tightly focused field is always purely linearly polarized and the longitudinal SAM annihilates in the focal plane. As a result, the SAM density is purely transverse in the focal plane, and the symmetry of the x and y components of the SAM density is the same as the patterns in Fig. 5. Additionally, the property of the evolution of SAM density is independent of the value of a, and the detailed illustration will not be discussed here.

We have presented the bipolar-variant SAM carried by VOF with complex singularities at the two fixed foci ($a = 0.3\rho_m$ on x axis) in a bipolar coordinate system; now we will study the case when the positions of the complex singularities are arbitrarily designed. We can rotate the bipolar coordinates to achieve general bipolar-variant SAM with arbitrary spatial distribution. Based on Eq. (1a), we can get the expression of the rotated bipolar coordinate u as

$$p^2 + (q - a\cot u)^2 = \frac{a^2}{\sin^2 u}, \tag{7}$$

where $p = x\cos\varphi_0 + y\sin\varphi_0$ and $q = -x\sin\varphi_0 + y\cos\varphi_0$, and φ_0 is the rotation angle of the bipolar coordinates in anticlockwise direction. In this case, the VOF carrying

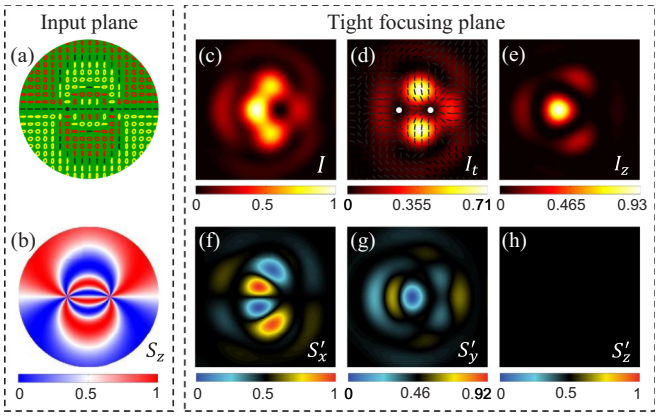

FIG. 6. (a) The polarization distribution and (b) longitudinal SAM density distribution of the VOF carrying bipolar-variant SAM with $m = 2$ and $a = 0.3\rho_m$ in the input plane. (c)–(e) The total intensity I, transverse intensity I_t, and longitudinal intensity I_z of the tightly focused VOF carrying bipolar-variant SAM in the tight focusing plane when NA = 0.95. The corresponding SoP is superimposed with the transverse intensity pattern in (d) and the white dots indicate polarization singularities. (f)–(h) Three components of the SAM density in the tight focusing plane. Any image in the focusing plane has a dimension of $3\lambda \times 3\lambda$.

general bipolar-variant SAM is $\mathbf{E} = \cos(mu)\hat{\mathbf{e}}_x + j\sin(mu)\hat{\mathbf{e}}_y$, and the two complex singularities of SAM locate at $(a\cos\varphi_0, a\sin\varphi_0)$ and $(-a\cos\varphi_0, -a\sin\varphi_0)$ in Cartesian coordinate system, respectively. The longitudinal SAM density of the VOF carrying general bipolar-variant SAM is $S_z = \frac{\varepsilon}{4\omega}\sin(2mu)$.

Figure 7 depicts the cases of rotated bipolar-variant SAM for $\varphi_0 = 0, \pi/8, \pi/4$ and $\pi/2$ when $m = 1$, $a = 0.5\rho_m$, respectively. It is clear that the SoP and the longitudinal SAM density S_z of the VOF carrying general bipolar-variant SAM rotate by the same rotation angle φ_0. The transverse SAM density S'_x and S'_y of the tightly focused field also exhibit anticlockwise rotation. When $\varphi_0 = 0$, S'_x is opposite about x axis and S'_y is the same about x axis, while S'_x is the same about y axis and S'_y is opposite about y axis when $\varphi_0 = \pi/2$. The two complex singularities of SAM change into two V points during the focusing process, which agrees with the above discussion. More interestingly, the amount of the singularities keeps topologically invariant in this process, and the positions of the singularities also rotate along with the rotation angle φ_0.

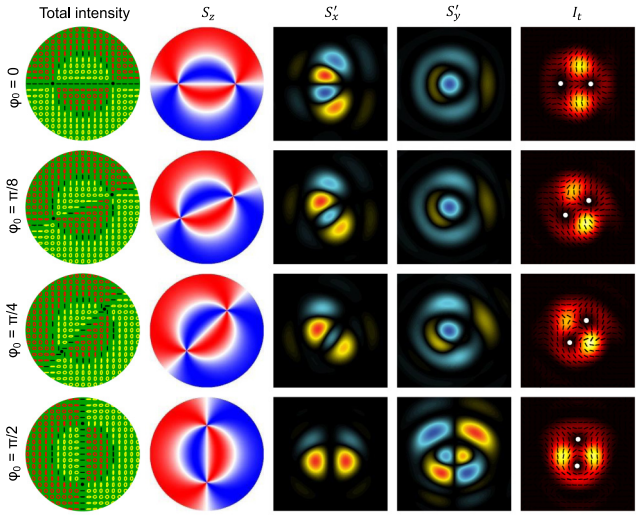

FIG. 7. The SoP and longitudinal SAM density of the VOF carrying general bipolar-variant SAM with $a = 0.5\rho_m$ and $m = 1$ are shown in the first two columns, and the x and y components of the SAM density in the focal plane with NA = 0.95 are shown in third and fourth columns, respectively. The transverse intensity patterns of the tightly focused field are shown in the fifth column, and the corresponding SoPs are superimposed with the intensity patterns and the white dots indicate polarization singularities. The four rows show the four cases for the rotation angles of $0, \pi/8, \pi/4$ and $\pi/2$, respectively. Any image in the focusing plane has a dimension of $3\lambda \times 3\lambda$.

IV. THEORETICAL EXPLANATION FOR THE FOCAL EVOLUTION OF BIPOLAR-VARIANT SAM

To theoretically explain the annihilation of longitudinal SAM density and the appearance of transverse SAM density in the focusing process, we further analyze the schematic of the bipolar-variant SAM in input plane, as shown in Fig. 1(d). We notice that the variant SAMs around the two singularities may counteract with each other in focusing process, leading to the annihilation of longitudinal SAM density. For the VOF carrying bipolar-variant SAM, we can derive from Eqs. (1a) and (2) that the electric fields at the central symmetric positions are the complex conjugate of each other, which satisfies $\mathbf{E}(\rho, \varphi) = \mathbf{E}^*(\rho, \pi + \varphi)$. To calculate the tightly focused field originating from the input VOF at central symmetric positions, we choose to use a point-to-point theoretical analysis method to analyze the tightly focused field [45]. In this case, the Richards-Wolf vectorial diffraction integral in Eqs. (5) and (6) can be rewritten

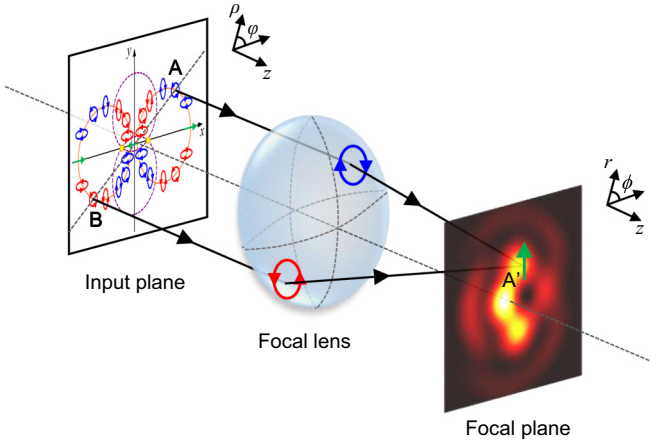

FIG. 8. Schematic illustration of the polarization evolution of the VOF carrying bipolar-variant SAM in the tight focusing process. Red ellipse: right-handed elliptic (circular) polarization; blue ellipse: left-handed elliptic (circular) polarization; green arrow: linear polarization.

in cylindrical coordinates as

$$\mathbf{E}(r,\phi,z) = -\frac{jk}{2\pi}\int_0^{\rho_m} d\rho \int_0^{2\pi} \begin{bmatrix} (E_x(\cos\theta\cos^2\varphi + \sin^2\varphi) + E_y\sin\varphi\cos\varphi(\cos\theta - 1))\hat{e}_x \\ (E_x\sin\varphi\cos\varphi(\cos\theta - 1) + E_y(\cos\theta\sin^2\varphi + \cos^2\varphi))\hat{e}_y \\ (E_x\cos\varphi\sin\theta + E_y\sin\varphi\sin\theta)\hat{e}_z \end{bmatrix} e^{jQ}\sin\theta/\sqrt{\cos\theta}d\varphi, \tag{8}$$

where (ρ, φ) are the radial and azimuthal coordinates in the incident plane. (r, ϕ) are the radial and azimuthal coordinates in the focal plane. $Q = k[z\cos\theta + r\sin\theta\cos(\phi - \varphi)]$, and $z = 0$ in the focal plane. The incident field is a round field with a radius of $\rho_m = f\mathrm{NA}$, where NA is the numerical aperture of the focal lens.

Based on the analysis method [45], we can choose two area elements A and B at the central symmetric positions without loss of generality, as shown in Fig. 8. The incident VOF in area elements $A(\rho, \varphi)$ and $B(\rho, \pi + \varphi)$ are $\mathbf{E}_A = \cos(u_A)\hat{\mathbf{e}}_x + j\sin(u_A)\hat{\mathbf{e}}_y$ and $\mathbf{E}_B = \cos(u_A)\hat{\mathbf{e}}_x - j\sin(u_A)\hat{\mathbf{e}}_y$, respectively. In this way, the contribution of the incident fields in the area elements A and B to the tightly focused field at arbitrary point $A'(r, \phi)$ in the focal plane should be

$$\Delta E_x(A') = -\frac{jk}{\pi}[\cos(mu_A)\cos Q(\cos\theta\cos^2\varphi + \sin^2\varphi) - \sin(mu_A)\sin Q\sin\varphi\cos\varphi(\cos\theta - 1)]\sin\theta/\sqrt{\cos\theta}\Delta\rho\Delta\varphi, \tag{9a}$$

$$\Delta E_y(A') = -\frac{jk}{\pi}[\cos(mu_A)\cos Q\sin\varphi\cos\varphi(\cos\theta - 1) - \sin(mu_A)\sin Q(\cos\theta\sin^2\varphi + \cos^2\varphi)]\sin\theta/\sqrt{\cos\theta}\Delta\rho\Delta\varphi, \tag{9b}$$

$$\Delta E_z(A') = \frac{k}{\pi}[\cos(mu_A)\sin Q\cos\varphi + \sin(mu_A)\cos Q\sin\varphi]\sin^2\theta/\sqrt{\cos\theta}\Delta\rho\Delta\varphi. \tag{9c}$$

From Eqs. (9), it can be seen that the x component of the tightly focused VOF carrying bipolar-variant SAM at point A' is in phase with the y component, giving rise to the annihilation of longitudinal SAM density. Meanwhile, the z component and $x(y)$ component of the tightly focused field are always $\pm\pi/2$ out of phase. In this way, the tightly focused field is elliptically or circularly polarized in the meridional plane depending on the relative amplitudes of the two components, leading to a purely transverse SAM density in the focal plane. Thus, we can draw the conclusion that the variant SAMs around the two singularities counteract with each other in focusing process, leading to the annihilation of longitudinal SAM and the appearance of transverse SAM. We should state that this method is valid by choosing area elements in the input plane to analyze the tightly focused field, because the integral calculation is essentially summation and the group of area elements in the input plane is chosen arbitrarily. As the above conclusions are drawn on the basis of the fact that the incident VOF is with bipolar-variant longitudinal SAM distribution, we believe that the purely transverse SAM density in the focal plane is induced by the bipolar-variant longitudinal SAM. In addition, similar conclusion can also be drawn for the general bipolar-variant SAM with Eq. (7), which will not be discussed in detail here. We should also point out that besides the evolution property of the bipolar-variant SAM in a tight focusing process, it would also be interesting to explore its transition in nonlinear interaction or light-matter interaction [46,47].

V. CONCLUSION

To conclude, we have theoretically and experimentally presented the bipolar-variant SAM carried by the VOF and concentrated on studying the spatial evolution of the bipolar-variant SAM during the tight focusing process, finding that the longitudinal SAM density annihilates and the purely transverse SAM density appears in the focal plane. Moreover, we further studied the SAM evolution of the general bipolar-variant SAM and found that the amount of singularities keeps topological invariance when the complex singularities of SAM change into V points after tight focusing. We reported three kinds of transitions in the tight focusing process: (i) from purely longitudinal SAM to purely transverse SAM, (ii) from hybrid SoP to pure linear SoP in the transverse plane, and (iii) from complex singularities of SAM to V points. We believe the concepts in this paper can inspire ideas in designing space-variant SAM distribution as well as enriching the family of VOFs, and the study of evolution properties can provide insight into optical angular momentum and singular optics. This paper also provides a way to generate purely transverse SAM density induced by longitudinal SAM, which may be applied in optical trapping and manipulation, especially for optically induced rotations.

ACKNOWLEDGMENTS

National Natural Science Foundation of China (11804187, 11904199); Natural Science Foundation of Shandong Province (ZR2019BF006); A Project of Shandong Province Higher Educational Science and Technology Program (J18KA229).

[1] M. Padgett and R. Bowman, Nat. Photon. **5**, 343 (2011).
[2] L. Allen, M. W. Beijersbergen, R. J. C. Spreeuw, and J. P. Woerdman, Phys. Rev. A **45**, 8185 (1992).
[3] L. Allen, M. J. Padgett, and M. Babiker, Prog. Opt. **39**, 291 (1999).
[4] Y. Zhao, J. S. Edgar, G. D. M. Jeffries, D. McGloin, and D. T. Chiu, Phys. Rev. Lett. **99**, 073901 (2007).
[5] B. Sephton, A. Dudley, and A. Forbes, Appl. Opt. **55**, 7830 (2016).
[6] Y. Lei, X. Xu, N. Wang, and H. Jia, J. Opt. **20**, 105701 (2018).

[7] M. E. J. Friese, T. A. Nieminen, N. R. Heckenberg, and H. Rubinsztein Dunlop, Nature **394**, 348 (1998).

[8] A. Lehmuskero, R. Ogier, T. Gschneidtner, P. Johansson, and M. Kall, Nano Lett. **13**, 3129 (2013).

[9] A. Aiello, N. Lindlein, C. Marquardt, and G. Leuchs, Phys. Rev. Lett. **103**, 100401 (2009).

[10] K. Y. Bliokh, A. Y. Bekshaev, and F. Nori, Nat. Commun. **5**, 3300 (2014).

[11] A. Aiello, P. Banzer, M. Neugebauer, and G. Leuchs, Nat. Photon. **9**, 789 (2015).

[12] M. Neugebauer, T. Bauer, A. Aiello, and P. Banzer, Phys. Rev. Lett. **114**, 063901 (2015).

[13] M. Li, S. Yan, Y. Liang, P. Zhang, and B. Yao, Phys. Rev. A **95**, 053802 (2017).

[14] A. Canaguier-Durand and C. Genet, Phys. Rev. A **89**, 033841 (2014).

[15] K. Y. Kim and S. Kim, Opt. Lett. **41**, 135 (2016).

[16] M. Li, S. Yan, B. Yao, Y. Liang, and P. Zhang, Opt. Express **24**, 20604 (2016).

[17] Q. Zhan, Adv. Opt. Photon. **1**, 1 (2009).

[18] H. Rubinsztein-Dunlop, A. Forbes, M. V. Berry, M. R. Dennis, D. L. Andrews, M. Mansuripur, C. Denz, C. Alpmann, P. Banzer, T. Bauer *et al.*, J. Opt. **19**, 013001 (2017).

[19] A. Ohtsu, Y. Kozawa, and S. Sato, Appl. Phys. B **98**, 851 (2010).

[20] C. Chang, Y. Gao, J. Xia, S. Nie, and J. Ding, Opt. Lett. **42**, 3884 (2017).

[21] R. Chen, Z. Chen, Y. Gao, J. Ding, and S. He, Laser Photon. Rev. **11**, 1700165 (2017).

[22] E. Otte, C. Alpmann, and C. Denz, Laser Photon. Rev. **12**, 1700200 (2018).

[23] P. Shi, L. Du, and X. Yuan, Opt. Express **26**, 23449 (2018).

[24] A. K. Singh, S. Saha, S. D. Gupta, and N. Ghosh, Phys. Rev. A **97**, 043823 (2018).

[25] W. Zhu, V. Shvedov, W. She, and W. Krolikowski, Opt. Express **23**, 34029 (2015).

[26] Y. Guan, L. Zhong, C. Qian, and R. Chen, Appl. Sci. **9**, 960 (2019).

[27] G. M. Lerman, L. Stern, and U. Levy, Opt. Express **18**, 27650 (2010).

[28] X. L. Wang, Y. Li, J. Chen, C. S. Guo, J. Ding, and H. T. Wang, Opt. Express **18**, 10786 (2010).

[29] A. M. Beckley, T. G. Brown, and M. A. Alonso, Opt. Express **18**, 10777 (2010).

[30] G. Milione, H. I. Sztul, D. A. Nolan, and R. R. Alfano, Phys. Rev. Lett. **107**, 053601 (2011).

[31] Y. Pan, Y. Li, S. M. Li, Z. C. Ren, Y. Si, C. Tu, and H. T. Wang, Opt. Lett. **38**, 3700 (2013).

[32] B. Gu, B. Wen, G. Rui, Y. Xue, Q. Zhan, and Y. Cui, Opt. Lett. **41**, 1566 (2016).

[33] K. Y. Bliokh, A. Y. Bekshaev, and F. Nori, Phys. Rev. Lett. **119**, 073901 (2017).

[34] L. Han, S. Liu, P. Li, Y. Zhang, H. Cheng, and J. Zhao, Phys. Rev. A **97**, 053802 (2018).

[35] P. Yu, Q. Zhao, X. Hu, Y. Li, and L. Gong, Opt. Lett. **43**, 5677 (2018).

[36] Z. Cui, J. Sun, N. M. Litchinitser, and Y. Han, J. Opt. **21**, 015401 (2019).

[37] X. L. Wang, J. Ding, W. J. Ni, C. S. Guo, and H. T. Wang, Opt. Lett. **32**, 3549 (2007).

[38] X. L. Wang, J. Chen, Y. Li, J. Ding, C. S. Guo, and H. T. Wang, Phys. Rev. Lett. **105**, 253602 (2010).

[39] Y. Pan, Y. Li, Z. C. Ren, Y. Si, C. Tu, and H. T. Wang, Phys. Rev. A **89**, 035801 (2014).

[40] X. Z. Gao, Y. Pan, S. M. Li, D. Wang, Y. Li, C. Tu, and H. T. Wang, Phys. Rev. A **93**, 033834 (2016).

[41] M. S. Soskin and M. V. Vasnetsov, Prog. Opt. **42**, 219 (2001).

[42] M. R. Dennis, K. O'Holleran, and M. J. Padgett, Prog. Opt. **53**, 293 (2009).

[43] B. Richards and E. Wolf, Proc. Roy. Soc. A **253**, 358 (1959).

[44] K. S. Youngworth and T. G. Brown, Opt. Express **7**, 77 (2000).

[45] Y. Pan, Z. C. Ren, L. J. Kong, C. H. Tu, Y. N. Li, and H. T. Wang, Opt. Express **28**, 23416 (2020).

[46] Y. Kozawa and S. Sato, J. Opt. Soc. Am. B **25**, 175 (2008).

[47] W. Zhang, J. Tang, Y. Ming, C. Zhang, and Y. Q. Lu, Opt. Express **28**, 2818 (2020).